

ECGFlowCMR: Pretraining with ECG-Generated Cine CMR Improves Cardiac Disease Classification and Phenotype Prediction

Xiaocheng Fang^{1,2*}, Zhengyao Ding^{3*}, Jieyi Cai^{1,4}, Yujie Xiao¹, Bo Liu², Jiarui Jin^{1,2}, Haoyu Wang^{1,4}, Guangkun Nie², Shun Huang¹, Ting Chen⁵, Hongyan Li^{2†}, and Shenda Hong^{1†}

¹ National Institute of Health Data Science, Peking University, China

² School of Intelligence Science and Technology, Peking University, China

³ College of Computer Science and Technology, Zhejiang University, China

⁴ University of Chinese Academy of Sciences, China

⁵ The First Affiliated Hospital of Zhejiang University School of Medicine, China

{hongshenda, leehy}@pku.edu.cn

Abstract. Cardiac Magnetic Resonance (CMR) imaging provides a comprehensive assessment of cardiac structure and function but remains constrained by high acquisition costs and reliance on expert annotations, limiting the availability of large-scale labeled datasets. In contrast, electrocardiograms (ECGs) are inexpensive, widely accessible, and offer a promising modality for conditioning the generative synthesis of cine CMR. To this end, we propose ECGFlowCMR, a novel ECG-to-CMR generative framework that integrates a Phase-Aware Masked Autoencoder (PA-MAE) and an Anatomy-Motion Disentangled Flow (AMDF) to address two fundamental challenges: (1) the cross-modal temporal mismatch between multi-beat ECG recordings and single-cycle CMR sequences, and (2) the anatomical observability gap due to the limited structural information inherent in ECGs. Extensive experiments on the UK Biobank and a proprietary clinical dataset demonstrate that ECGFlowCMR can generate realistic cine CMR sequences from ECG inputs, enabling scalable pretraining and improving performance on downstream cardiac disease classification and phenotype prediction tasks. The code is available at <https://github.com/PKUDigitalHealth/ECGFlowCMR>.

Keywords: ECG-to-CMR Generation · Cross-Modal Synthesis · Phase Awareness · Anatomy-Motion Disentanglement · Generative Pretraining

1 Introduction

Cardiac Magnetic Resonance (CMR) imaging is a pivotal noninvasive modality for the comprehensive assessment of cardiac structure and function [2,22]. However, the development of AI models for automated CMR analysis is hindered by the scarcity of large-scale, expertly annotated datasets. Although the UK Biobank (UKB) [4] provides 42,129 CMR scans, this scale remains significantly

* Equal contribution.

†Corresponding author: Shenda Hong and Hongyan Li.

below the sample size (typically on the order of 10^5 to 10^6) required to pretrain robust foundation models [1,14]. The substantial cost and annotation burden associated with CMR acquisition have so far precluded the release of larger public datasets, thereby limiting the generalizability and clinical utility of AI-based methods. In this context, generative modeling has emerged as a promising approach to synthesize realistic CMR data at scale, mitigating data scarcity and enhancing model performance.

Recent advances in generative AI have enabled high-fidelity synthesis across a range of medical imaging modalities, including chest X-rays [3,17], 3D brain MRIs [16,19], and echocardiogram videos [5,11], thereby enhancing representation learning and downstream task performance. In contrast, CMR synthesis remains relatively underexplored. For example, DragNet [24] generates cine CMR sequences from a single static frame, but its performance is constrained by frame-wise conditioning, which fails to capture spatiotemporal coherence. CPGG [12] conditions generation on cardiac phenotypes derived from CMR via segmentation and quantification, creating a circular dependency on expert-annotated CMR data and limiting scalability. These limitations highlight the need for more flexible and annotation-free generative paradigms tailored to CMR synthesis.

Given the limited availability of CMR data, a natural and scalable direction is to synthesize cine CMR sequences conditioned on electrocardiograms (ECGs), a low-cost and widely accessible modality routinely acquired in both clinical practice and population-scale screening. ECGs capture rich electrophysiological dynamics that correlate with cardiac structure and function [25], thereby providing a promising surrogate signal for scalable data-driven modeling. Early explorations of ECG-to-CMR translation include the cross-modal autoencoder proposed by Radhakrishnan et al. [18], which embeds ECG and MRI into a shared latent space to enable direct imputation of CMR sequences from ECG inputs. CardioNets [6] further introduces a masked autoregressive model (MAR) that generates cine CMR in a latent space conditioned on ECG signals. Collectively, these studies establish the feasibility of ECG-to-CMR synthesis.

However, ECG-to-CMR synthesis faces two key challenges: **1) Cross-modal temporal mismatch:** A 10-second ECG captures multi-beat electrophysiological dynamics with variable heart rates, whereas a 50-frame cine CMR typically represents a single, phase-resolved cardiac cycle. This discrepancy renders temporal alignment and beat-to-cycle correspondence inherently ambiguous, complicating sequence generation. **2) Anatomical observability gap:** As ECG primarily reflects surface-level electrical activity rather than structural morphology, it imposes only weak constraints on cardiac anatomy and image appearance. This under-constrained mapping often results in synthetic CMRs that capture coarse motion patterns but fail to reconstruct fine-grained anatomical details.

To address these challenges, we propose ECGFlowCMR, a generative framework that integrates the Phase-Aware Masked Autoencoder (PA-MAE) and the Anatomy-Motion Disentangled Flow (AMDF). PA-MAE learns ECG representations under dual supervision from signal reconstruction and phase prediction, identifying complete cardiac cycles via a dedicated phase head to temporally

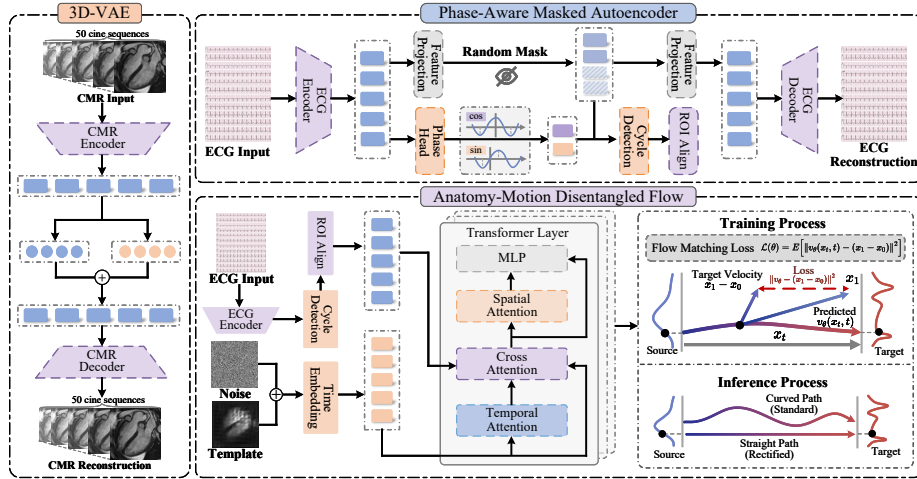


Fig. 1: Illustration of our proposed ECGFlowCMR, which integrates PA-MAE and AMDF to synthesize realistic cine CMR sequences from 12-lead ECGs.

align with cine CMR sequences. AMDF first derives a time-invariant anatomical anchor using a 3D variational autoencoder (3D-VAE), yielding a static latent template which serves as a structural prior. Conditioned on this template and an initial motion state, a Diffusion Transformer (DiT)-based flow-matching network predicts ECG-conditioned velocity fields to jointly refine anatomical structure and synthesize temporally coherent motion. Extensive experiments on the UK Biobank and a proprietary clinical dataset demonstrate that ECGFlowCMR generates realistic cine CMR sequences from ECGs, enabling scalable pretraining and improving performance on downstream cardiac analysis tasks.

2 Methodology

2.1 Phase-Aware Masked Autoencoder

To extract semantically rich and rhythm-aware representations from 12-lead ECGs, we propose the Phase-Aware Masked Autoencoder (PA-MAE). Trained with dual supervision, PA-MAE facilitates robust morphological representation learning and enables precise temporal alignment with cine CMR sequences.

Masked Signal Reconstruction. As shown in Fig. 1, PA-MAE adopts a standard masked autoencoder [8] for self-supervised ECG representation learning. Given an input ECG, the encoder extracts semantic features from partially masked sequences. The decoder reconstructs the original signal, and the model is trained using mean squared error (MSE) between input and reconstruction. This promotes the extraction of morphological patterns without manual annotations.

Phase-Aware Temporal Supervision. In parallel, a dedicated phase prediction head \mathcal{P} maps the unmasked encoder features to a sinusoidal representation of the cardiac phase:

$$\hat{\phi} = \mathcal{P}(\mathbf{f}) = [\sin(\phi), \cos(\phi)], \quad (1)$$

where $\phi \in [0, 2\pi]$ denotes the normalized phase within each cardiac cycle. Ground-truth phase labels ϕ_{gt} are computed via R-peak detection from Lead II and linearly interpolated across each R-R interval. The phase prediction loss is followed:

$$\mathcal{L}_{\text{phase}} = \frac{1}{T'} \|\hat{\phi} - \phi_{\text{gt}}\|_2^2. \quad (2)$$

Here, T' denotes the temporal length after encoding. To temporally align ECG with cine CMR, complete cardiac cycles are identified from the predicted phase sequence, and each cycle is resampled using ROI Align into a 50-frame representation, matching the temporal resolution of cine CMR.

Training Objective. The overall training objective combines both reconstruction and phase prediction losses:

$$\mathcal{L}_{\text{PA-MAE}} = \mathcal{L}_{\text{rec}} + \mathcal{L}_{\text{phase}}. \quad (3)$$

This dual-supervision strategy ensures the learned features preserve both morphological and temporal semantics essential for downstream CMR synthesis.

2.2 Anatomy-Motion Disentangled Flow

To address the anatomical observability gap where ECG signals impose weak constraints on cardiac morphology, we propose the Anatomy-Motion Disentangled Flow (AMDF), which explicitly disentangles static anatomical structure from dynamic temporal motion in a latent space.

Anatomical Anchor Learning. We first train a 3D variational autoencoder (3D-VAE) [10] to encode cine CMR sequences into a temporally coherent latent space. This latent space compresses spatial anatomy while preserving temporal continuity. After training, we compute the mean latent across all sequences to derive a static anatomical template, which captures population-level cardiac morphology and serves as a structural prior.

Conditional Flow Matching. Conditioned on the anatomical template and an initial motion state, a Diffusion Transformer (DiT)-based flow-matching network [15,13] learns continuous velocity fields that model time-varying motion. Specifically, we define a velocity field $v_{\theta}(\mathbf{z}_t, t, \mathbf{c})$ that governs the temporal evolution of the latent representation, where \mathbf{z}_t is the interpolated latent at time $t \in [0, 1]$, and \mathbf{c} denotes ECG features extracted by the PA-MAE encoder.

During training, we sample $t \sim \mathcal{U}(0, 1)$ and construct a latent interpolation between the noise-injected template \mathbf{z}_0 and the target CMR latent \mathbf{z}_1 as:

$$\mathbf{z}_t = (1 - t) \cdot \mathbf{z}_0 + t \cdot \mathbf{z}_1, \quad \mathbf{z}_0 = \mathbf{z}_{\text{template}} + \alpha \cdot \boldsymbol{\epsilon}, \quad \boldsymbol{\epsilon} \sim \mathcal{N}(0, \mathbf{I}). \quad (4)$$

Here, \mathbf{z}_1 is encoded by the 3D-VAE and α controls the noise scale. The ground-truth velocity field is defined as the constant drift between the two states:

$$\mathbf{v}_{\text{true}} = \mathbf{z}_1 - \mathbf{z}_0. \quad (5)$$

The network v_{θ} predicts the velocity field conditioned on the interpolated latent state, time, and ECG features:

$$\hat{\mathbf{v}} = v_{\theta}(\mathbf{z}_t, t, \mathbf{c}). \quad (6)$$

Table 1: Comparison with geneartive approaches on the UKB dataset.

Method	LPIPS \downarrow	FID \downarrow	FVD \downarrow	Inference time \downarrow
VideoGPT [23]	0.35	107.41	24.99	2.15 sec / vid.
ModelScopeT2V [21]	0.37	104.19	31.43	3.87 sec / vid.
CardioNets [6]	0.28	89.83	21.65	4.33 sec / vid.
EchoPulse [11]	0.31	85.80	21.41	0.84 sec / vid.
Ours	0.27	37.28	14.41	0.45 sec / vid.

Table 2: Comparison of different methods on cardiac disease classification.

Methods	UKB-CAD		UKB-CM		UKB-HF	
	ACC	AUC	ACC	AUC	ACC	AUC
ViT [7]	0.662 \pm 0.014	0.714 \pm 0.022	0.705 \pm 0.008	0.747 \pm 0.032	0.708 \pm 0.038	0.779 \pm 0.018
MAE [8](real)	0.695 \pm 0.086	0.743 \pm 0.048	0.776 \pm 0.017	0.806 \pm 0.054	0.776 \pm 0.032	0.854 \pm 0.016
<i>Training with 100% Mixed Synthetic Data</i>						
VideoGPT [23]	0.697 \pm 0.045	0.752 \pm 0.021	0.779 \pm 0.051	0.809 \pm 0.038	0.781 \pm 0.025	0.857 \pm 0.012
ModelScopeT2V [21]	0.701 \pm 0.031	0.761 \pm 0.052	0.784 \pm 0.024	0.811 \pm 0.042	0.784 \pm 0.054	0.859 \pm 0.031
CardioNets [6]	0.706 \pm 0.054	0.769 \pm 0.018	0.792 \pm 0.037	0.819 \pm 0.014	0.791 \pm 0.009	0.861 \pm 0.045
EchoPulse [11]	0.709 \pm 0.012	0.778 \pm 0.035	0.799 \pm 0.007	0.828 \pm 0.048	0.798 \pm 0.032	0.868 \pm 0.019
Ours	0.716\pm0.027	0.787\pm0.011	0.806\pm0.035	0.837\pm0.024	0.808\pm0.018	0.876\pm0.026
<i>Training with 200% Mixed Synthetic Data</i>						
VideoGPT [23]	0.699 \pm 0.028	0.765 \pm 0.044	0.788 \pm 0.019	0.815 \pm 0.052	0.789 \pm 0.041	0.856 \pm 0.025
ModelScopeT2V [21]	0.705 \pm 0.051	0.774 \pm 0.015	0.796 \pm 0.044	0.823 \pm 0.031	0.797 \pm 0.012	0.864 \pm 0.053
CardioNets [6]	0.711 \pm 0.036	0.782 \pm 0.027	0.804 \pm 0.022	0.831 \pm 0.015	0.804 \pm 0.048	0.871 \pm 0.037
EchoPulse [11]	0.717 \pm 0.014	0.789 \pm 0.058	0.810 \pm 0.053	0.839 \pm 0.029	0.811 \pm 0.026	0.878 \pm 0.014
Ours	0.723\pm0.019	0.796\pm0.028	0.818\pm0.013	0.845\pm0.039	0.817\pm0.030	0.886\pm0.021
<i>Training with 300% Mixed Synthetic Data</i>						
VideoGPT [23]	0.709 \pm 0.034	0.776 \pm 0.051	0.798 \pm 0.042	0.825 \pm 0.016	0.800 \pm 0.054	0.863 \pm 0.032
ModelScopeT2V [21]	0.714 \pm 0.047	0.783 \pm 0.023	0.805 \pm 0.014	0.833 \pm 0.051	0.807 \pm 0.021	0.870 \pm 0.044
CardioNets [6]	0.718 \pm 0.025	0.790 \pm 0.048	0.812 \pm 0.033	0.841 \pm 0.027	0.813 \pm 0.045	0.877 \pm 0.019
EchoPulse [11]	0.723 \pm 0.052	0.797 \pm 0.013	0.818 \pm 0.028	0.848 \pm 0.054	0.820 \pm 0.012	0.884 \pm 0.036
Ours	0.730\pm0.011	0.804\pm0.033	0.826\pm0.020	0.854\pm0.014	0.826\pm0.028	0.891\pm0.016

The training objective minimizes the mean squared error (MSE) between the predicted and ground-truth velocity fields:

$$\mathcal{L}_{\text{AMDF}} = \mathbb{E}_{t, \mathbf{z}_0, \mathbf{z}_1, \mathbf{c}} [\|\mathbf{v}_\theta(\mathbf{z}_t, t, \mathbf{c}) - (\mathbf{z}_1 - \mathbf{z}_0)\|_2^2]. \quad (7)$$

Inference and Sampling. At inference time, we synthesize cine CMR latents by integrating the learned velocity field from \mathbf{z}_0 to \mathbf{z}_1 via Euler integration:

$$\mathbf{z}_{t+\Delta t} = \mathbf{z}_t + \Delta t \cdot \mathbf{v}_\theta(\mathbf{z}_t, t, \mathbf{c}). \quad (8)$$

The final latent \mathbf{z}_1 is decoded by the 3D-VAE to generate cine CMR sequences. AMDF jointly refines anatomical structure and synthesizes ECG-guided temporal motion, thereby effectively addressing the anatomical observability gap.

3 Experiments

3.1 Experiments Setting

We evaluated ECGFlowCMR on four-chamber cine CMR sequences from **the UK Biobank (UKB)**, comprising 42,129 samples split into 29,490/4,212/8,427

Table 3: Comparison of different methods on cardiac phenotype prediction.

Methods	LVEDV		LVEF		LVM		RVEDV		Overall	
	MAE	R ²	MAE	R ²	MAE	R ²	MAE	R ²	R ²	
ViT [7]	11.52	0.772	3.75	0.367	7.56	0.763	13.14	0.770	0.417	
MAE [8] (real)	11.35	0.769	3.67	0.412	6.67	0.801	12.62	0.784	0.441	
<i>Training with 100% Mixed Synthetic Data</i>										
VideoGPT [23]	11.20	0.773	3.54	0.415	6.48	0.805	12.47	0.786	0.445	
ModelScopeT2V [21]	11.28	0.771	3.51	0.418	6.51	0.808	12.40	0.790	0.443	
CardioNets [6]	10.97	0.782	3.47	0.423	6.32	0.814	12.25	0.799	0.451	
EchoPulse [11]	10.83	0.785	3.44	0.427	6.25	0.818	12.16	0.802	0.454	
Ours	10.40	0.806	3.41	0.436	6.14	0.828	11.92	0.809	0.470	
<i>Training with 200% Mixed Synthetic Data</i>										
VideoGPT [23]	11.24	0.774	3.51	0.417	6.44	0.806	12.49	0.789	0.447	
ModelScopeT2V [21]	11.25	0.773	3.45	0.421	6.35	0.812	12.27	0.795	0.452	
CardioNets [6]	10.82	0.791	3.43	0.429	6.24	0.817	12.04	0.803	0.459	
EchoPulse [11]	10.69	0.795	3.40	0.433	6.14	0.821	11.89	0.806	0.463	
Ours	10.19	0.812	3.39	0.441	5.92	0.836	11.53	0.821	0.482	
<i>Training with 300% Mixed Synthetic Data</i>										
VideoGPT [23]	11.13	0.778	3.47	0.420	6.39	0.809	12.42	0.791	0.450	
ModelScopeT2V [21]	11.18	0.775	3.42	0.425	6.31	0.815	12.20	0.797	0.456	
CardioNets [6]	10.65	0.798	3.38	0.434	6.17	0.821	11.84	0.808	0.465	
EchoPulse [11]	10.44	0.804	3.36	0.435	6.04	0.826	11.79	0.811	0.471	
Ours	9.97	0.821	3.32	0.442	5.84	0.844	11.32	0.834	0.499	

for training/validation/testing at the patient level. For disease classification, we constructed three case cohorts: cardiomyopathy (UKB-CM, n=196), coronary artery disease(UKB-CAD, n=5,464), and heart failure(UKB-HF, n=578), each with a 1:1 ratio of positive and negative cases. For cardiac phenotype prediction, we subset the above split to 19,487/2,758/5,553 samples with complete annotations for 82 phenotypes, following the UKB protocol [2]. To evaluate generalization, we further assessed model performance on **a proprietary clinical dataset collected from the Affiliated Hospital of Zhejiang University**. This independent cardiomyopathy dataset comprises 535 subjects and is used for two downstream tasks: (1) binary classification of cardiomyopathy versus control, and (2) four-class classification of cardiomyopathy subtypes. Specifically, the dataset includes 195 cases of hypertrophic cardiomyopathy (HCM), 160 of dilated cardiomyopathy (DCM), 33 of restrictive cardiomyopathy (RCM), and 147 healthy controls. All classification tasks were evaluated using five-fold cross-validation. Evaluation metrics included LPIPS [26], FID [9], FVD [20], and inference time.

For data preprocessing, we employed the UKB segmentation model [2] to extract cardiac regions and resized all CMR videos to $1 \times 50 \times 96 \times 96$. A 3D-VAE was trained to encode videos with $8 \times$ spatial compression, while our PA-MAE was used to process 12-lead ECGs with 5,000 timepoints, $8 \times$ downsampling, and a 0.5 random mask ratio. Our AMDF was trained with AdamW ($\text{lr}=1 \times 10^{-4}$, weight decay= 1×10^{-4} , batch size=4) for 10 epochs, and downstream models were fine-tuned for 100 epochs. All experiments were performed on an NVIDIA A100 GPU. We compared against four state-of-the-art baselines: VideoGPT [23], ModelScopeT2V [21], CardioNets [6], and EchoPulse [11].

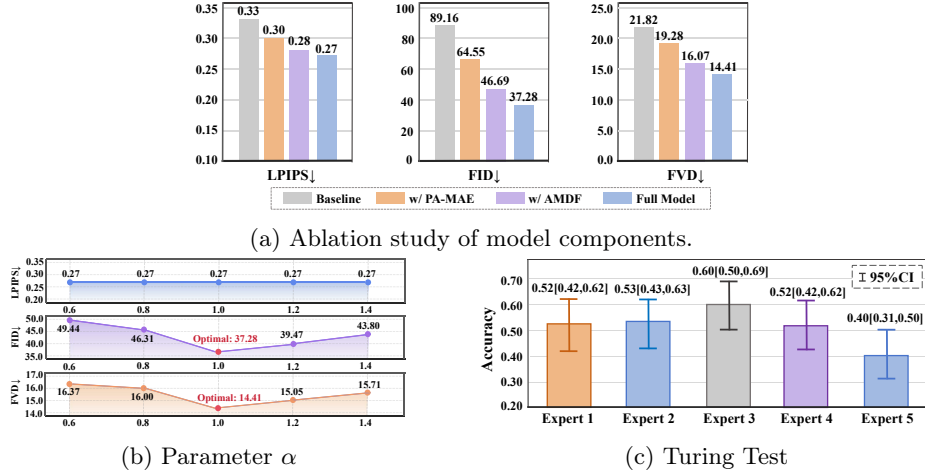


Fig. 2: Ablation study, parameter analysis, and turing test on the UKB dataset.

3.2 Comparisons with State-of-The-Arts

Evaluation on CMR Generation Quality. As shown in Table 1, our method outperforms prior generative baselines on UKB, achieving consistent gains in both perceptual and distributional fidelity. Specifically, it yields lower LPIPS (0.27 vs. 0.28), substantially reduces FID (37.28 vs. 85.80) and FVD (14.41 vs. 21.41), and achieves faster inference speed (0.45 s vs. 0.84 s per video).

Evaluation on Disease Classification. Table 2 presents classification results on three UKB case cohorts under 100%/200%/300% synthetic-data mixing. Our method consistently achieves the highest ACC and AUC across all tasks, with performance improving steadily as more synthetic data are incorporated.

Evaluation on Cardiac Phenotypes Prediction. Table 3 reports the prediction results for several important phenotypes and the average R^2 across 82 cardiac phenotypes under 100%/200%/300% synthetic-data mixing. Across all ratios, our method consistently achieves the lowest errors and highest R^2 , with overall performance improving as more synthetic data are introduced.

3.3 Ablation Studies and Parameter Analysis

We conduct a systematic ablation study to quantify the contribution of each module in ECGFlowCMR on the UKB dataset. As shown in Fig. 2a, removing any individual component leads to consistent performance degradation, demonstrating that the modules are complementary and jointly essential for optimal performance. We further analyze the sensitivity to the noise scale hyperparameter α defined in Eq. 4. As shown in Fig. 2b, ECGFlowCMR achieves optimal performance at $\alpha = 1.0$.

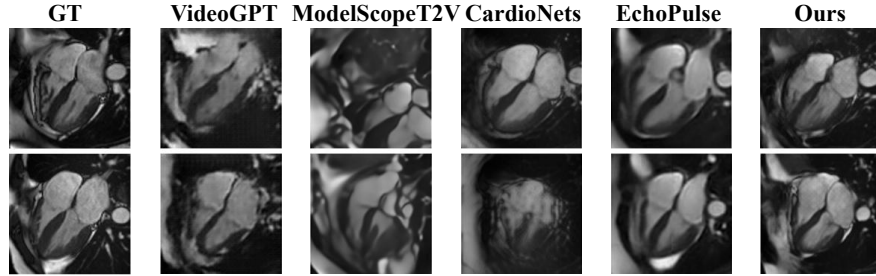


Fig. 3: Comparison of synthesized CMR frames across various models.

Table 4: Performance of our ECGFlowCMR in the private dataset.

Classification	Binary Classification		Four-Class Classification	
	Method	ACC	AUC	ACC
ViT [7]	0.736 \pm 0.038	0.671 \pm 0.061	0.531 \pm 0.022	0.694 \pm 0.055
MAE [8](real)	0.801 \pm 0.054	0.798 \pm 0.029	0.664 \pm 0.047	0.784 \pm 0.063
-mix 100%	0.804 \pm 0.039	0.813 \pm 0.041	0.687 \pm 0.052	0.814 \pm 0.028
-mix 200%	0.815 \pm 0.047	0.826 \pm 0.051	0.696 \pm 0.035	0.834 \pm 0.042
-mix 300%	0.836\pm0.027	0.843 \pm 0.029	0.717 \pm 0.054	0.853\pm0.026
-mix 400%	0.828 \pm 0.043	0.848\pm0.059	0.745\pm0.045	0.846 \pm 0.053
-mix 500%	0.818 \pm 0.052	0.838 \pm 0.037	0.733 \pm 0.041	0.837 \pm 0.055

3.4 External Validation and Qualitative Results

External Validation. To assess generalization beyond UKB, we evaluated ECGFlowCMR on a proprietary clinical dataset. As shown in Table 4, ACC and AUC improve consistently with more synthetic data, saturating at 300%–400% mixing ratios. Further augmentation to 500% may slightly degrade performance, indicating an optimal augmentation regime beyond which excessive mixing introduces distributional shift or redundancy that limits downstream utility.

Turing Test. We conducted a Turing Test with five cardiologists (one junior, three mid-level, and one senior) to assess the perceptual realism of ECGFlowCMR-synthesized cine CMR. Fifty real and fifty generated videos were randomly sampled, shuffled, and independently presented for binary real-versus-synthetic classification. As shown in Fig. 2c, the average accuracy was 0.514, indicating near-chance performance and suggesting that the synthesized CMR sequences are visually indistinguishable from real ones, even for experienced clinicians.

Visualization Results. Fig. 3 presents representative synthesized cine CMR frames from different generative models. Additional video comparisons are provided in the **supplementary material**.

4 Conclusion

In this paper, we propose ECGFlowCMR, a generative framework that synthesizes realistic cine CMR sequences from 12-lead ECGs by addressing two core

challenges: cross-modal temporal mismatch and anatomical observability gap. Integrating the PA-MAE and the AMDF modules, ECGFlowCMR enables scalable pretraining and improves downstream performance in cardiac classification and phenotype prediction. Extensive experiments on the UK Biobank and a proprietary clinical dataset demonstrate its quantitative and qualitative superiority over prior methods, highlighting its potential for data-efficient cardiac imaging.

References

1. Abbaspourazad, S., Elachqar, O., Miller, A., Emrani, S., Nallasamy, U., Shapiro, I.: Large-scale training of foundation models for wearable biosignals. In: ICLR (2024)
2. Bai, W., Suzuki, H., Huang, J., Francis, C., Wang, S., Tarroni, G., Guitton, F., Aung, N., Fung, K., Petersen, S.E., et al.: A population-based phenome-wide association study of cardiac and aortic structure and function. *Nature medicine* **26**(10), 1654–1662 (2020)
3. Bluethgen, C., Chambon, P., Delbrouck, J.B., Van Der Sluijs, R., Połacin, M., Zambrano Chaves, J.M., Abraham, T.M., Purohit, S., Langlotz, C.P., Chaudhari, A.S.: A vision–language foundation model for the generation of realistic chest x-ray images. *Nature Biomedical Engineering* **9**(4), 494–506 (2025)
4. Bycroft, C., Freeman, C., Petkova, D., Band, G., Elliott, L.T., Sharp, K., Motyer, A., Vukcevic, D., Delaneau, O., O’Connell, J., et al.: The uk biobank resource with deep phenotyping and genomic data. *Nature* **562**(7726), 203–209 (2018)
5. Chen, T., Shi, Y., Zheng, Z., Yan, B., Hu, J., Zhu, X.X., Mou, L.: Ultrasound image-to-video synthesis via latent dynamic diffusion models. In: MICCAI. pp. 764–774. Springer (2024)
6. Ding, Z., Li, Z., Hu, Y., Xu, Y., Zhao, C., Mao, Y., Li, H., Li, Z., Li, Q., Wang, J., et al.: Translating electrocardiograms to cardiac magnetic resonance imaging useful for cardiac assessment and disease screening: A multi-center study ai for ecg to cmr translation study. arXiv preprint arXiv:2411.13602 (2024)
7. Dosovitskiy, A.: An image is worth 16x16 words: Transformers for image recognition at scale. arXiv preprint arXiv:2010.11929 (2020)
8. He, K., Chen, X., Xie, S., Li, Y., Dollár, P., Girshick, R.: Masked autoencoders are scalable vision learners. In: CVPR. pp. 16000–16009 (2022)
9. Heusel, M., Ramsauer, H., Unterthiner, T., Nessler, B., Hochreiter, S.: Gans trained by a two time-scale update rule converge to a local nash equilibrium (2017)
10. Kingma, D.P., Welling, M.: Auto-encoding variational bayes. arXiv preprint arXiv:1312.6114 (2013)
11. Li, Y., Kim, S., Wu, Z., Jiang, H., Pan, Y., Jin, P., Song, S., Shi, Y., Yu, X., Yang, T., et al.: Echopulse: Ecg controlled echocardiogram video generation. In: ICLR (2025)
12. Li, Z., Hu, Y., Ding, Z., Mao, Y., Li, H., Yi, F., Zhang, H., Huang, Z.: Phenotype-guided generative model for high-fidelity cardiac mri synthesis: Advancing pre-training and clinical applications. In: MICCAI. pp. 484–494. Springer (2025)
13. Liu, X., Gong, C., et al.: Flow straight and fast: Learning to generate and transfer data with rectified flow. In: ICLR (2023)
14. Moor, M., Banerjee, O., Abad, Z.S.H., Krumholz, H.M., Leskovec, J., Topol, E.J., Rajpurkar, P.: Foundation models for generalist medical artificial intelligence. *Nature* **616**(7956), 259–265 (2023)

15. Peebles, W., Xie, S.: Scalable diffusion models with transformers. In: ICCV. pp. 4195–4205 (2023)
16. Peng, W., Adeli, E., Bosschieter, T., Park, S.H., Zhao, Q., Pohl, K.M.: Generating realistic brain mrис via a conditional diffusion probabilistic model. In: MICCAI. pp. 14–24. Springer (2023)
17. Prakash, E., Valanarasu, J.M.J., Chen, Z., Reis, E.P., Johnston, A., Pareek, A., Bluethgen, C., Gatidis, S., Olsen, C., Chaudhari, A.S., et al.: Evaluating and improving the effectiveness of synthetic chest x-rays for medical image analysis. In: ICCV. pp. 4413–4421 (2025)
18. Radhakrishnan, A., Friedman, S.F., Khurshid, S., Ng, K., Batra, P., Lubitz, S.A., Philippakis, A.A., Uhler, C.: Cross-modal autoencoder framework learns holistic representations of cardiovascular state. *Nature Communications* **14**(1), 2436 (2023)
19. Tudosiu, P.D., Pinaya, W.H., Ferreira Da Costa, P., Dafflon, J., Patel, A., Borges, P., Fernandez, V., Graham, M.S., Gray, R.J., Nachev, P., et al.: Realistic morphology-preserving generative modelling of the brain. *Nature Machine Intelligence* **6**(7), 811–819 (2024)
20. Unterthiner, T., Van Steenkiste, S., Kurach, K., Marinier, R., Michalski, M., Gelly, S.: Fvd: A new metric for video generation (2019)
21. Wang, J., Yuan, H., Chen, D., Zhang, Y., Wang, X., Zhang, S.: Modelscope text-to-video technical report. arXiv preprint arXiv:2308.06571 (2023)
22. Wang, Y.R., Yang, K., Wen, Y., Wang, P., Hu, Y., Lai, Y., Wang, Y., Zhao, K., Tang, S., Zhang, A., et al.: Screening and diagnosis of cardiovascular disease using artificial intelligence-enabled cardiac magnetic resonance imaging. *Nature Medicine* **30**(5), 1471–1480 (2024)
23. Yan, W., Zhang, Y., Abbeel, P., Srinivas, A.: Videogpt: Video generation using vq-vae and transformers. arXiv preprint arXiv:2104.10157 (2021)
24. Zakeri, A., Hokmabadi, A., Bi, N., Wijesinghe, I., Nix, M.G., Petersen, S.E., Frangi, A.F., Taylor, Z.A., Gooya, A.: Dragnet: Learning-based deformable registration for realistic cardiac mr sequence generation from a single frame. *Medical Image Analysis* **83**, 102678 (2023)
25. Zettinig, O., Mansi, T., Neumann, D., Georgescu, B., Rapaka, S., Seegerer, P., Kayvanpour, E., Sedaghat-Hamedani, F., Amr, A., Haas, J., et al.: Data-driven estimation of cardiac electrical diffusivity from 12-lead ecg signals. *Medical image analysis* **18**(8), 1361–1376 (2014)
26. Zhang, R., Isola, P., Efros, A.A., Shechtman, E., Wang, O.: The unreasonable effectiveness of deep features as a perceptual metric. In: CVPR. pp. 586–595 (2018)